JOURNAL GEOLOGICAL SOCIETY OF INDIA
Vol.97, November 2021, pp.1379-1386

Application of Microseismic Monitoring in Analysing the Stability of Underground Cavern

Vikalp Kumar[a,b,*], Prakash Chandra Jha[a], Nagendra Pratap Singh[b] and Sivakumar Cherukuri[a]

[a]National Institute of Rock Mechanics, Second stage Banashankari, Bengaluru - 560 070, India
[b]Department of Geophysics, Institute of Science, BHU, Varanasi - 221 005, India
***E-mail:** vikalpk@gmail.com*

ABSTRACT

Long term stability of an underground cavern is significant for construction engineers. For structures constructed in the geologically active regions of the Himalayas, continuous monitoring is required to ward off the sustained threats due to seismic activities and associated local geological hazards. Underground powerhouse of Tapovan Vishnugad Hydropower Power Project (TVHPP), Chamoli, Uttarakhand is one such powerhouse that encountered various types of rockmass failures both during and post construction. The project area is located about 2.0 km north of the Main Central Thrust (MCT) and the rockmass cavern has numerous joints, shear and seam zones and fractures. This pose threat to the long term stability of this underground powerhouse cavern. To analyse the rockmass stability of the powerhouse, real time microseismic monitoring system was installed in this underground cavern. Spatio-temporal variation of the recorded seismic events has been analysed for microseismic events distribution in terms of seismic energy, displacement, cumulative apparent volume and various other contours led to the identification of potentially hazardous zones in the underground rockmass structure.

INTRODUCTION

Tapovan Vishnugad Hydropower Project (4X130 MW) is impounded on the river Dhauli-Ganga in Chamoli, Uttarakhand, India. Underground powerhouse structure of this project is located on the bank of river Alaknanda (NTPC 2007). This underground excavation constructed under heavily stressed rockmass is at + 300 m depth and 2.0 km north of Main Central Thrust (MCT) (Dasgupta et al., 2000).

Rockburst, rockmass spalling occurred during and post excavation of TVHPP powerhouse. Excavation leads to increase stress level around the opening of various caverns (machine hall, transformer hall, Cable Ventilation Tunnel, Adit to Pressure Shaft etc.) that pose a threat to the life of manpower working in the powerhouse and enhanced the probability of damage to the machinery. Prediction of rockburst and rockmass spalling have been attempted to predict through the geotechnical equipment (Dunnicliff, 1982; Finno, 1991) but it did not provide sufficient information about the dynamic movement in the rockmass in near real time. Excavation in a rockmass generally increases the stress level which is redistributed in the surroundings (majority in the crown area and abutments) (Emsley et al., 1997; Martin et al., 2003). This stress redistribution generates micro-cracks in the rockmass which suddenly releases energy and is recorded as microseismic events (Chen et al., 2018). Stress redistribution has a tell-tale effect on excavated underground rockmass cavern. For the stability analysis of an underground powerhouse, microseismic monitoring system has been installed in various hydropower projects (Dai, Li, et al., 2015; Xiao et al., 2018; Li et al., 2019; Xiao, Li et al., 2019). So, a real time remote monitoring microseismic system was installed at TVHPP powerhouse for assessing the stability of TVHPP underground rockmass structure. This system was installed initially in 2013 with a limited coverage but later this was expanded in 2016 to cover the complete strata behaviour after excavation.

This paper discusses data analysis from the microseismic monitoring networking in terms of the stability of rockmass of the powerhouse.

TVHPP PROJECT DESCRIPTION

The underground powerhouse of TVHPP is situated at 30.54° N, 79.52° E in Chamoli, Uttarakhand, India. This powerhouse complex consists of thirteen number of major and minor tunnels (Fig.1). Major tunnels are main access tunnel, machine hall, transformer hall, tail race tunnel, adit to pressure shaft and cable ventilation tunnel and remaining others are minor tunnels. Major cavern/tunnels dimensions are listed in Table 1. Machine hall is separated by a distance of 55 m from transformer hall by two bus ducts, connecting tunnel and escape tunnel. Bus ducts, connecting tunnel and escape tunnels are D- shaped structure. Conventional drill and blast method was used for the construction of this underground powerhouse structure.

GEOLOGY OF THE AREA

Powerhouse of TVHPP is situated in the Alaknanda basin of Garhwal Lesser Himalaya (Vyshnavi et al., 2015) (Fig.2). This basin consists of following major lithotectonic units: STDS-South Tibetan detachment system, VT-Vaikrita thrust, MT-Munsiari thrust and RT-Ramgarh thrust. Underground powerhouse is about 2 km north and downward of Vaikrita thrust. Figure 3 shows the prominent shear seam and shear zone in this powerhouse cavern. Biotite schist occurs in and around the connecting tunnel. Rock mass between bus duct-1 and bus duct-2 also consists of this biotite schist. Rockmass in the powerhouse is mainly of medium to high grade metamorphic rocks. Exposed rocks are mainly quartzite, mica schists, fine grained quartz mica gneisses and augen gneisses which belong to Helang Formation of central crystalline. These rocks form prominent ridges in the area.

Foliation trend in the rockmass varies from N70° W – S 70° E to NW-SE having dips of 40° - 60° towards NE. There are three types of quartzite in the powerhouse - massive, jointed and highly jointed which have been divided based on joint characteristics and its spacing. The quarzitic rocks generally strike N70° W– S70° E and dip at 30°- 40° towards N20°E direction (Naithani and Murthy, 2006). A shear zone traverses in the crown of machine hall (1 m thick with 10 cm gouge) and passes in the zone of crown of the powerhouse. In addition to the shear zone, there are three bands of biotite schist along the

0016-7622/2021-97-11-1379/$ 1.00 © GEOL. SOC. INDIA | DOI: 10.1007/s12594-021-1876-y

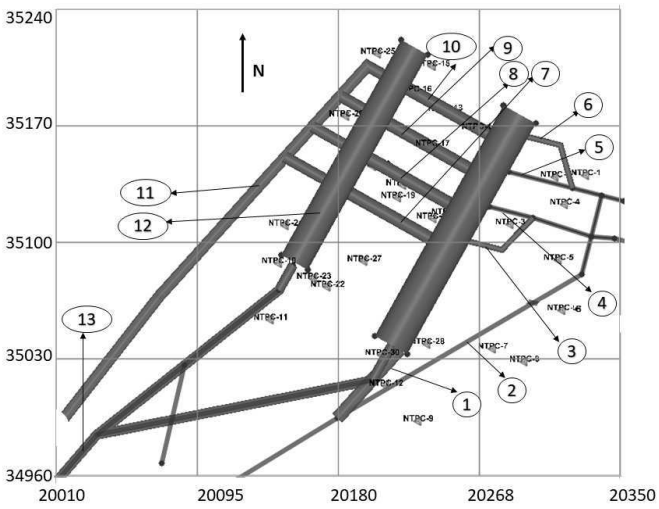

Fig.1. TVHPP Powerhouse complex layout with 3D visualization of installed geophone locations (1: Main access tunnel, 2: Adit to Pressure Shaft, 3: UPS-1, 4: UPS-2, 5: UPS-3, 6: UPS-4, 7: Connecting Tunnel, 8: Bus duct-1, 9: Bus duct-2,10: Escape tunnel, 11: Tail race tunnel, 12: Transformer hall and 13: Cable ventilation tunnel).

foliation joint (J1) which intersect the machine hall between 75 mm and 110 m chainage and transformer hall between 14.0m to 33.0m chainage.

MICROSEISMIC MONITORING SYSTEM AT TVHPP

Reconnaissance survey was conducted for identification of geophone and data acquisition unit (seismic station) locations and cable layout; body wave (longitudinal and transverse) velocities and media attenuation characteristics were also determined (Xu *et al.* 2010). On the basis of this reconnaissance survey, three-dimensional microseismic monitoring network consisting mainly of thirty geophones and ten data acquisition units (DAQ) also known as seismic stations were installed at the powerhouse cavern to record the waveform generated by the occurrence of micro-cracks in and around the TVHPP powerhouse (Fig. 4). DAQ unit digitizes, time stamp and perform the operation of triggering and validation of the recorded waveforms transferred from geophone using armored copper shield cable. Raw waveforms from DAQ units are further transferred to the communication equipment kept in the underground laboratory using armour-copper shield cable. Underground laboratory consists of desktop run time system (DRTS) having data acquisition and processing software. The recorded data are further transferred to NIRM, Bengaluru using the web for manual processing and interpretation. Table 2 lists the geophone locations (northing, easting and elevation) and its identity index.

Table 1. Excavation dimension in TVHPP powerhouse

Sl. No.	Tunnel	Length (m)	Width (m)	Height (m)
1	Machine hall	158.50	22.30	25.87
2	Transformer hall	147.75	18.00	27.65
3	Escape Tunnel	55.00	3.00	3.00
4	Bus Duct (both)	55.00	12.00	11.50
5	Connecting Tunnel	55.00	8.00	8.00
6	Cable ventilation tunnel	289.21	6.00	6.00
7	Main Access Tunnel	294.00	8.00	6.00
8	Adit to pressure shaft	245.10	6.00	8.00
9	Unit pen stock 1 and 4	45.81	6.00	7.50
10	Unit pen stock 2	27.33	6.00	7.50
11	Unit pen stock 3	39.76	6.00	7.50
12	Tail Race Tunnel (TRT)	355.00	7.00	7.00

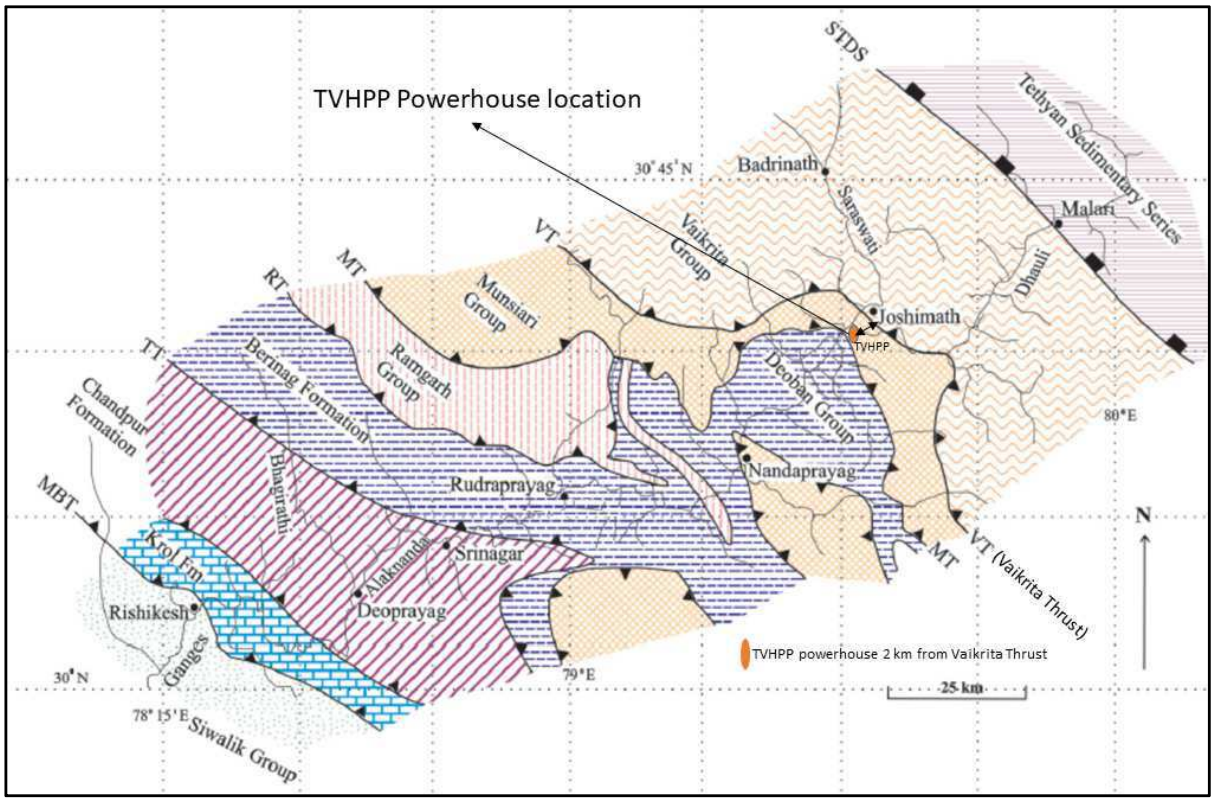

Fig.2. Geological map of the Alaknanda section of Garhwal Lesser Himalaya showing various lithotectonic units of the Himalaya STDS-South Tibetan detachment system, VT-Vaikrita Thrust, MT-Munsiari Thrust, RT-Ramgarh Thrust, TVHPP powerhouse is marked in Orange dot and at a distance of 2 km from Vaikrita Thrust.

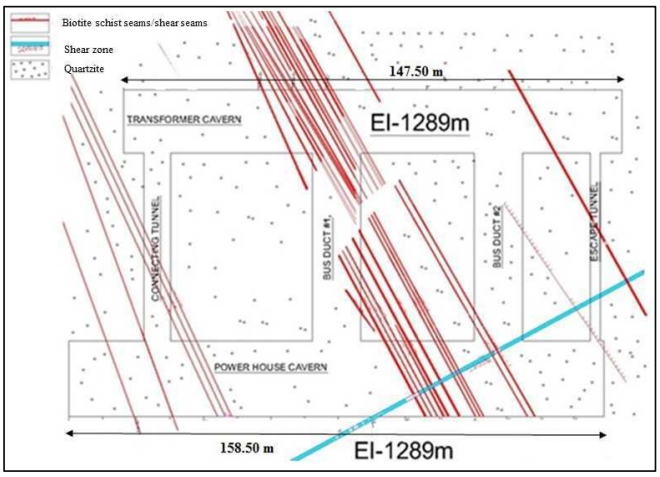

Fig.3. Shear sand seam zone of powerhouse

Source location and its time of occurrence are calculated using P and S wave arrival and source parameters from wave form analysis (Bormann et al. 2009). The local magnitude at TVHPP is calculated by using the following equation (Glazer, 2018):

$$M_L = a\log_{10}(\text{energy}) + b\log_{10}(moment) + C$$

Where a, b and c are constants and has to be calculated during the calibration.

Microseismic monitoring at TVHPP started in 2013. After calibration run in 2013, the respective values of a, b and c are found to be 0.344, 0.516 and -6.594 respectively. Due to the site constraints, the operation was shut down in June 2013 and operation resumed again from 17 March 2016 and continued till 26 October 2016 for 224 days.

Acquired data is recorded and auto processed for only those triggered waveforms for which ratio of short term average to long term average (STA/LTA) exceeds a pre-defined threshold value and which are recorded by minimum of four geophones. Blasting were performed at different locations inside the cavern to find the P and S wave velocities. Various seismic parameters used for recording of microseismic events after the calibration of the site ground rock mass

Table 2. Geophone identity index and its location

S. No	Co-ordinate (in m)		
	Northing	Easting	Elevation
NTPC-1	35140.5	20328.2	1284.11
NTPC-2	35139.5	20309.8	1269.01
NTPC-3	35111.1	20282.62	1283.94
NTPC-4	35123	20315.41	1278.12
NTPC-5	35089.6	20311.66	1284.84
NTPC-6	35060.1	20317.56	1288.21
NTPC-7	35036.24	20272.05	1293.36
NTPC-8	35028.51	20291.06	1289.52
NTPC-9	34992.8	20227.13	1299.73
NTPC-10	35087.7	20143.14	1321.07
NTPC-11	35053.8	20138.16	1302.28
NTPC-12	35014.1	20207.76	1316.55
NTPC-13	35179.41	20243.51	1288.85
NTPC-14	35168.29	20263.67	1297.13
NTPC-15	35206.1	20235.8	1295.07
NTPC-16	35190.92	20224.78	1296.35
NTPC-17	35158.25	20235.67	1299.1
NTPC-18	35134.6	20218.05	1288.7
NTPC-19	35127.03	20214.92	1292.71
NTPC-20	35117.12	20245.43	1290.7
NTPC-21	35114.52	20236.22	1284.59
NTPC-22	35073.53	20172.41	1293.25
NTPC-23	35078.41	20164.22	1297.5
NTPC-24	35110.37	20147.13	1295.9
NTPC-25	35213.55	20202.8	1288.23
NTPC-26	35176.08	20183.7	1288.76
NTPC-27	35088.88	20194.63	1289.42
NTPC-28	3503910	20232.57	1293.3
NTPC-29	35145.91	20199.94	1282.67
NTPC-30	35032.45	20205.4	1321.01

conditions in the powerhouse area are as follows:

STA/LTA = 8

P wave velocity = 3.85 km/s

S wave velocity = 2.4 km/s

Picking error in P-wave = 1 ms and

Picking error in S-wave = 2 ms

Recorded waveforms consist of microseismic events as well as various electrical, mechanical, hammering, rockmass slide near by

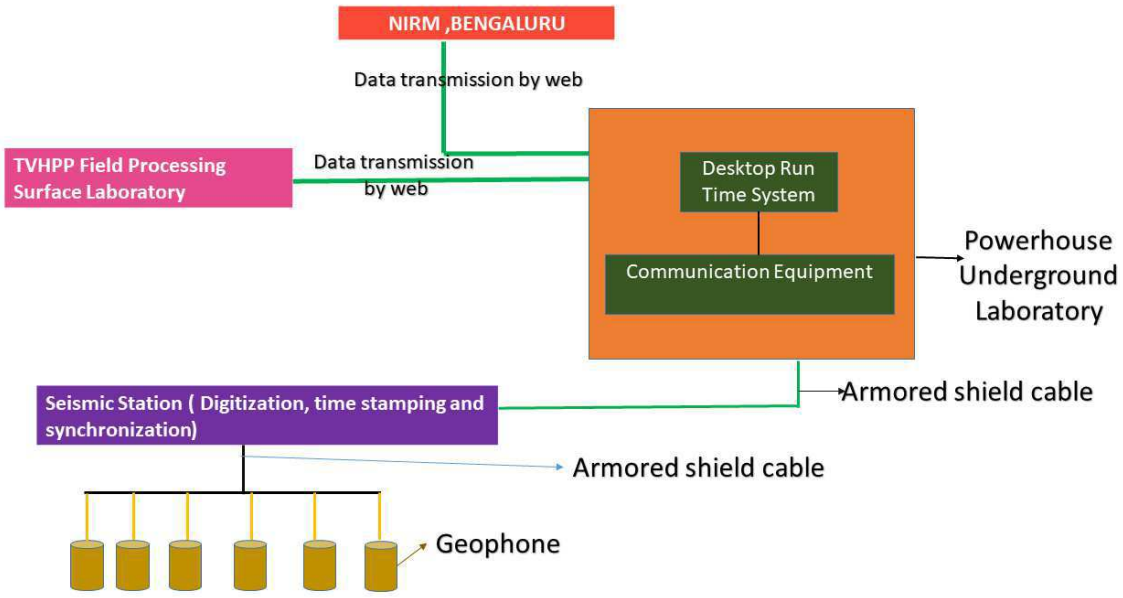

Fig.4. Microseismic Monitoring System layout at TVHPP.

and various other types of noises. Using waveform and frequency analysis, recorded waveforms are manually processed and micro-seismic events form the database of the accepted trigger waveforms. Microseismic events have normally high frequency content above 500 Hz, high amplitude and time duration is normally less than 1.0 s. Electrical noise has frequency of the order of 50 Hz and tremors have travel time difference between P and S wave is more than 50 ms and time duration is also higher (greater than 1 s). Maximum hypocentral location error percentage of microseismic event is 3% with absolute maximum error margin of 8.5 m.

It was considered that this network at TVHPHP would timely assess the stability and apparent stress re-distribution in and around the underground powerhouse cavern. In such a close-in monitoring network, formation of microseismic event clusters may indicate the zone in which micro-cracking is occurring (Essrich, 2005).

TEMPORAL ANALYSIS OF MICROSEISMIC EVENTS IN AND AROUND TVHPP POWERHOUSE

After filtering out the noises from recorded waveforms, 178 events were found as genuine microseismic events (Fig.5). This amounted to an average of 24 events per month. The impact of these events on the stability of the underground powerhouse cavern with time needs evaluation using various seismological parameters like seismic moment, seismic energy, cumulative displacement, cumulative apparent volume (CAV), Log_{10} energy index (EI), Gutenberg-Richter relationship.

Seismic moment can be calculated from fault slip dimensions sizes measured in field and analysis of seismic wave properties generated by the micro-cracks (frequency spectrum analysis) (Madariaga, 1989). Seismic energy is the amount of energy release during fracture and frictional sliding that results in the transformation of elastic strain into inelastic strain. Both the parameters, seismic moment and energy

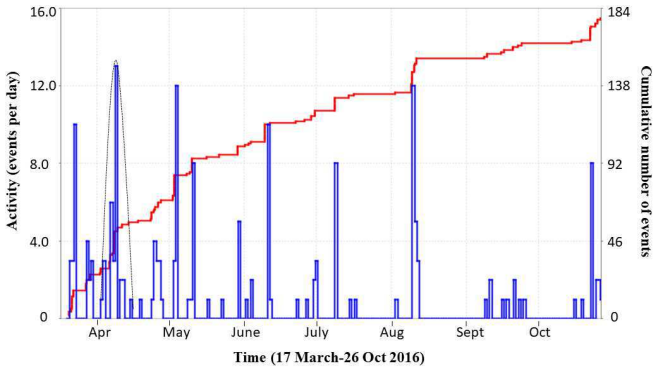

Fig.5. Activity (events per day) vs. Cumulative number of events

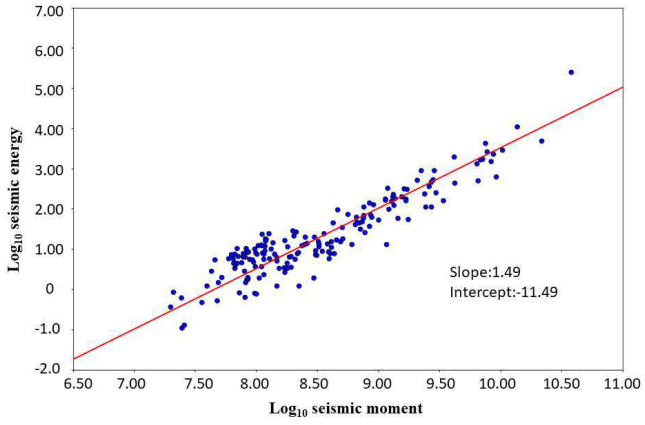

Fig.6. Log seismic energy vs log seismic moment

are inverted from the instrument, distance and scattering effect corrections of each waveform and then averaged. Radiated seismic energy normally increases with increase in the seismic moment on the log-log plot of both the parameters (Fig.6). The slope of this log-log linear relationship tells about the status of the cavern rockmass. If source of a microseismic event is associated with a softer patch in the rockmass or weak geological feature, such source produces larger seismic moment and radiate less seismic energy and results in low value of gradient. The opposite applies to a microseismic source which is associated with a strong geological feature or hard patch in the rockmass (Mendecki et al. 2010). Lower the gradient, softer the rockmass i.e. less energy is required for same amount of deformation. In this source, gradient is higher, i.e., more seismic energy is required per unit deformation. For this TVHPP underground powerhouse, gradient is 1.49 and intercept is -11.49. As this gradient is high, so, it implies that the deformation has decreased with time. Thus, it indicates a stable underground powerhouse rockmass cavern.

Energy Index (EI) is a tool to compare the radiated energies of microseismic events of similar potency (Aswegen and Butler 1993). The energy index of a seismic event is the ratio of the observed radiated seismic energy of that event to the average energy radiated by events of the observed seismic potency derived from the log-log plot of energy and potency. Higher the energy index, higher the driving stress at the source of the event at its time of occurrence. Figure 7 shows the plot of variations of cumulative displacement, cumulative apparent volume (CAV), Log_{10} Energy Index (EI) with time. Log_{10} EI first increases and then decreases in April 2016. This illustrates a process of accumulation and release of energy (loading and unloading) which results in the sudden increase of cumulative apparent volume. As the energy index increases, it indicates the driving stress on the powerhouse is increasing. This driving force was increasing the seismic activity rate in April 2016 (see Fig.5). This driving force may increase at such a value that it resulted in two microseismic events of higher local magnitude 0.7 and 0 on 3rd May 2016 that resulted in the sudden increase of cumulative displacement and correspondingly cumulative apparent volume.

The rate of micro-crack occurrence in TVHPP powerhouse cavern rockmass may be expressed by the Gutenberg-Richter relationship (Gutenberg and Richter 1956) (Fig.8)

$$\log_{10} N = a - b\, M_L \qquad (1)$$

where N=cumulative number of seismic events having local magnitude $M_L \geq m_{min}$, $a = \log_{10} N$ when $M_L = 0$ and b = slope of the semi-log plot between number of events N and local magnitude M_L. The parameter b represents the relationship between the number of small and large microseismic events. It is directly related with redistribution of stress due to excavation induced seismicity (Caving and Potvin, 2008; Hudyma, 2008). The respective values of "a" and

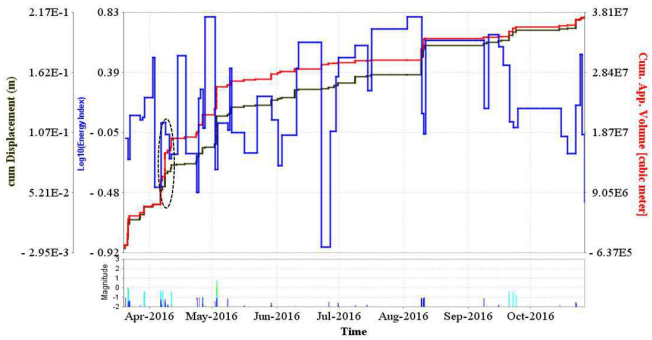

Fig.7. Variation of cumulative displacement, log (Energy Index) and Cumulative Apparent Volume (CAV) with time.

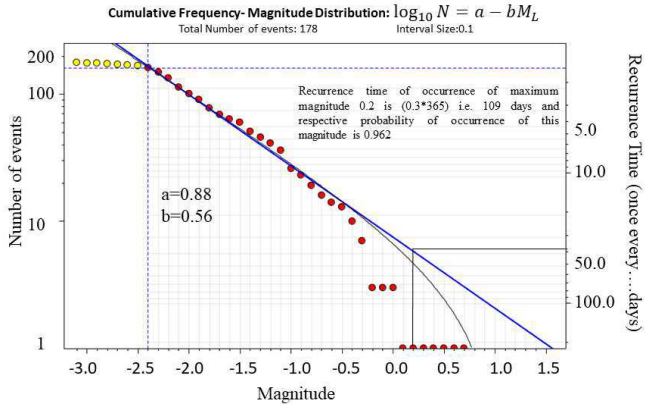

Fig.8. Gutenberg Richter relationship

"b" are 0.88 and 0.56 during the monitoring period. The number of microseismic events during Feb-June 2013 was 2254 and the b-value was 1.41 (Vikalp Kumar et al. 2019). As number of micro-cracks decreases with time, this results in the lower b-value with time.

One important parameter that can be derived from this semi-log plot is mean recurrence time T_r above events of certain size which can be calculated using the following equation (Mendecki, 2012):

$$T_r (\geq \mathrm{m}) = \Delta t / N (\geq \mathrm{m}) \quad (2)$$

where N is the number of microseismic events ≥ local magnitude m over monitoring rockmass volume, Δt is the period of monitoring. Recurrence time is appropriate when driving forces are relatively constant. As no blast was being carried out in the powerhouse during the monitoring period so that internal constant driving forces due to the composition of rockmass may be assumed to act only.

The largest seismic event m_{max} would have a local magnitude that corresponds to N ($\geq m_{max}$) = 1, or log1 = a – b m_{max} = 0, thus m_{max} = a/b, or

$$m_{max} = m_{min} + (1/b) \log N (\geq m) \quad (3)$$

Thus, the ratio a/b in equation (3) gives an estimate of the upper magnitude m_{max} which is a useful parameter for quantifying seismicity for this TVHPP underground powerhouse. This m_{max} is however only a relative maximum, limited to the size of the database used for 224 days and 178 events. As the respective value of parameter- a and b are 0.88 and 0.56, so, magnitude of largest seismic event m_{max} to be expected in one year is about 1.60.

Recurrence time of this maximum magnitude 1.60 is 234 days using equation (2). But in field data, maximum computed local magnitude microseismic event is 0.70. So, if the data were recorded for longer period, there is a probability to occur seismic event of magnitude 1.60 every year. So, occurrence of such high seismic magnitude in and around the powerhouse may damage the structure. So, advance precautions are required to handle such high magnitude events.

The probability that a seismic event would already have occurred or any future conditional occurrence probability can be estimated. The empirical probability P_t that in a given volume of rockmass V, an event of magnitude greater than m within a specific time after the occurrence of event of similar size can be calculated using the following equation (Mendecki, 2015):

$$P_t = (n_T + 1) / (n + 2) \quad (4)$$

where n is observed recurrence intervals Tr (≥m) , of which n_T are smaller than or equal to T.

Further recurrence time of various local magnitude may be computed and tabulated (Table 3) which shows the local magnitude from -0.9 to observed maximum magnitude 0.7 along with its probability for time period varies from two weeks to one year. Figure 9 illustrates this tabulated relationship between probability vs mean recurrence days for local magnitudes of microseismic events from -0.9 to 0.7. It is evident that as local magnitude increases, mean recurrence time increases and the probability of the corresponding events decreases. For example, local magnitude of microseismic event 0.7 takes 73 days to recur and its probability to occur in two weeks is 0.17 while event having local magnitude -0.9 takes 9 days to recur and its probability to occur in two weeks is 0.77. At the same time, for a microseismic event of definite local magnitude, probability increases as time increases. For example, probability of event of local magnitude -0.1 increases from 0.41 in two weeks to 0.99 in six months. Therefore, microseismic events of lower magnitude recur frequently than the higher local magnitude events and its probability also increases and for the event of same local magnitude, probability of occurrence increases as time duration increases.

SPATIAL DISTRIBUTION OF MICROSEISMIC EVENTS

Microseismic events is illustrated over three dimensional volume (430 m*430 m*193 m) in and around the powerhouse (Fig.10). The orientation of powerhouse structure in three dimensional view in south, west and downward directions are shown by red, green and blue arrows respectively. Size and colour of events are expressed in terms of $\log_{10}$ (energy).

Events of maximum local magnitude (0.7) and correspondingly having highest magnitude is about 50 m away the boundary of the end of the machine hall. Event count contour (ECC) is plotted for events from zero to 30 at contour interval of five (Fig.11). Dark blue line (ECC: 0) is at the boundary of monitoring volume while light blue line (ECC: 5) crosses transformer hall, APS and machine hall. Maximum event count contour (ECC:30, orange colour) occurred between connecting and bus duct-1 adjacent to the downstream wall of the machine hall/powerhouse chamber.

Displacement contour varies from zero to 15.90 m at contour interval of 2.65 (Fig.12). Though the occurrences of maximum microseismic event and correspondingly maximum event count contour is adjacent to the downstream wall of the machine hall between connecting tunnel and bus duct-1, but maximum displacement count contour is not in the same zone. Maximum induced displacement is noticed at about 50 m away from the end of the machine hall i.e., because events of higher magnitude had taken place in that zone.

Table 3. Probability table and Recurrence Times for various local magnitude

Local Magnitude	-0.9	-0.7	-0.5	-0.3	-0.1	0.1	0.3	0.5	0.7
Mean recurrence days	9	12	16	20	26	34	44	57	73
Pr (2weeks)	0.77	0.68	0.58	0.49	0.41	0.33	0.27	0.21	0.17
Pr (1month)	0.96	0.91	0.85	0.76	0.67	0.58	0.49	0.40	0.33
Pr (3 months)	1.00	0.99	0.99	0.99	0.96	0.92	0.86	0.79	0.67
Pr (6 months)	1.00	1.00	1.00	1.00	0.99	0.99	0.98	0.96	0.91
Pr (1year)	1.00	1.00	1.00	1.00	1.00	1.00	1.00	0.99	0.99

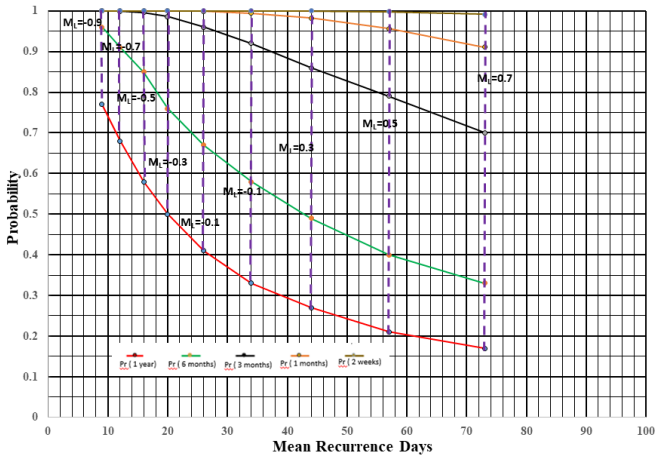

Fig.9. Probability vs. mean recurrence days of microseismic events of local magnitude Ml from -0.9 to 0.7

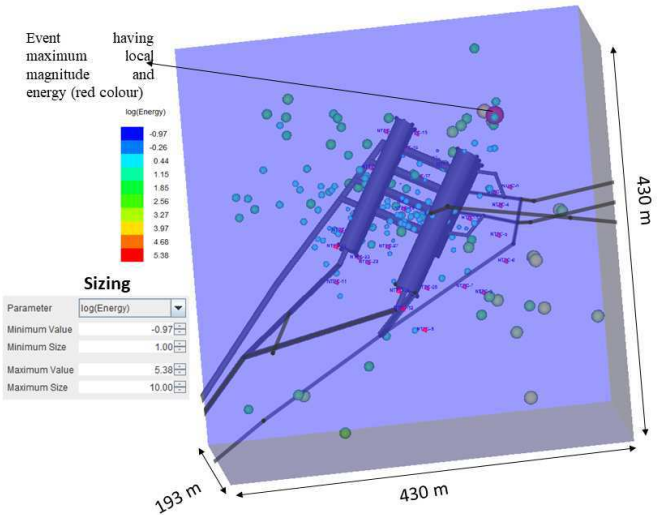

Fig.10. Three dimensional Monitoring volume of TVHPP cavern

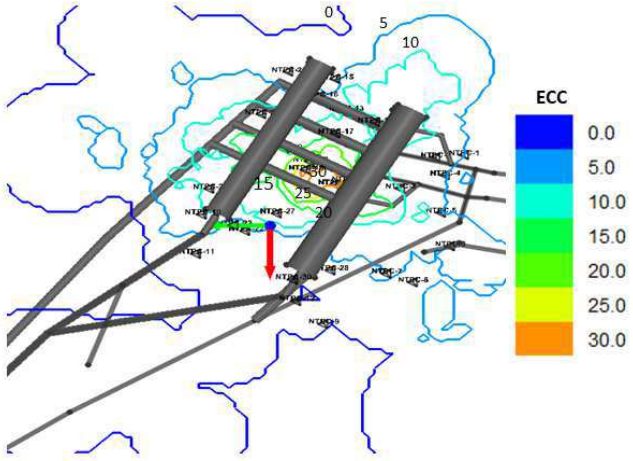

Fig.11. Event count contour (ECC)

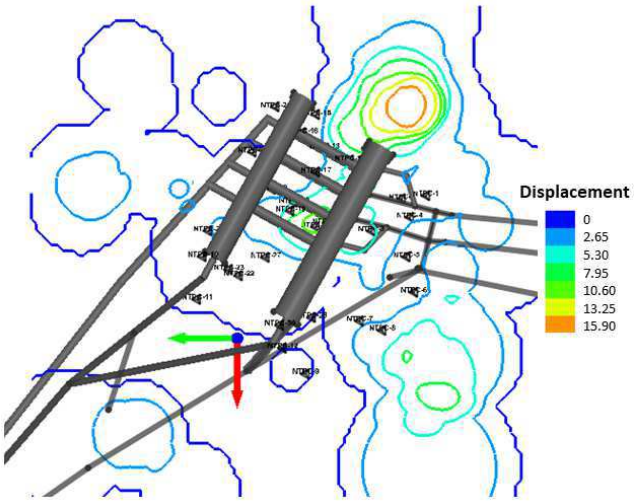

Fig.12. Displacement contour

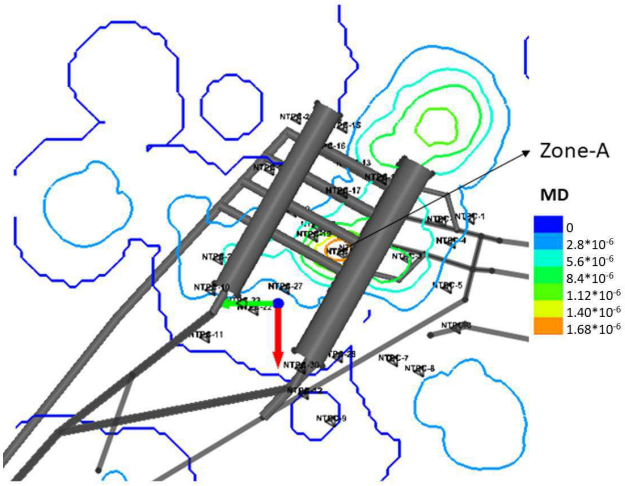

Fig.13. Mcgarr Displacement (MD)

Mcgarr displacement is associated with events having average slip D over a smaller fault zone of source radius of the events .Small scale seismic moment corresponding to the asperity failure is expressed by (Mcgarr, 1991)

$$D = M / (\mu\pi r^2) \quad (5)$$

where M = seismic moment, μ = modulus of rigidity and r = source radius.

Thus, Mcgarr displacement for a given rockmass depends mainly on event source radius and seismic moment. Over an identified zone, if large number of low magnitude microseismic events occur, these low magnitude events may coalescence and that may be interpreted in terms of high Mcgarr displacement and further may result in the failure of that zone of rockmass over monitoring volume.

Figure 13 illustrates Mcgarr Displacement (MD) contour that varies from zero (dark blue colour) to $1.68*10^{-5}$ (orange colour) at contour interval of $2.8*10^{-6}$. Minimum MD contour (dark blue colour) is at the boundary of monitoring volume while next level MD contour of $2.8*10^{-6}$ (light blue colour) passes through machine hall, transformer hall, both the bus ducts, escape tunnel. Maximum MD contour ($1.68*10^{-5}$) occurs in the rockmass between connecting tunnel and bus duct-1 and is designated as zone -A. Thus, it indicates that a macro crack is forming in this zone-A (Daulat 2007; Mcgarr and Fletcher, 2003). This may be due to occurrences of more number of microseismic events in this zone.

CORRELATION WITH GEOLOGICAL SETTING

If local fault orientation or shear rockmass favours for slip under present stress conditions, micro-crack or fracture growth in the shear

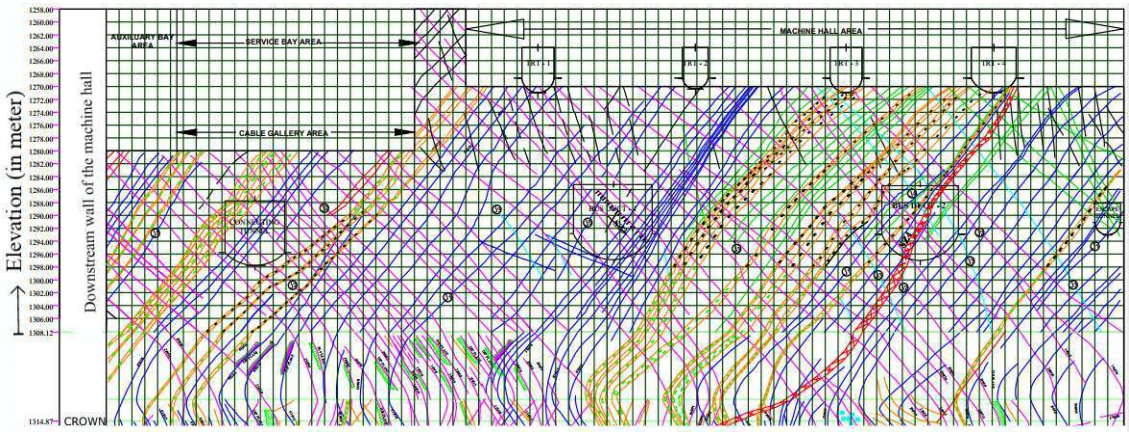

Fig.14. Geological log downstream wall of the machine hall showing Joints: J1, J2, J3, J4 and J5; Shear Zone: SZ1, SZ2, SZ3, SZ4, SZ5 and SZ6

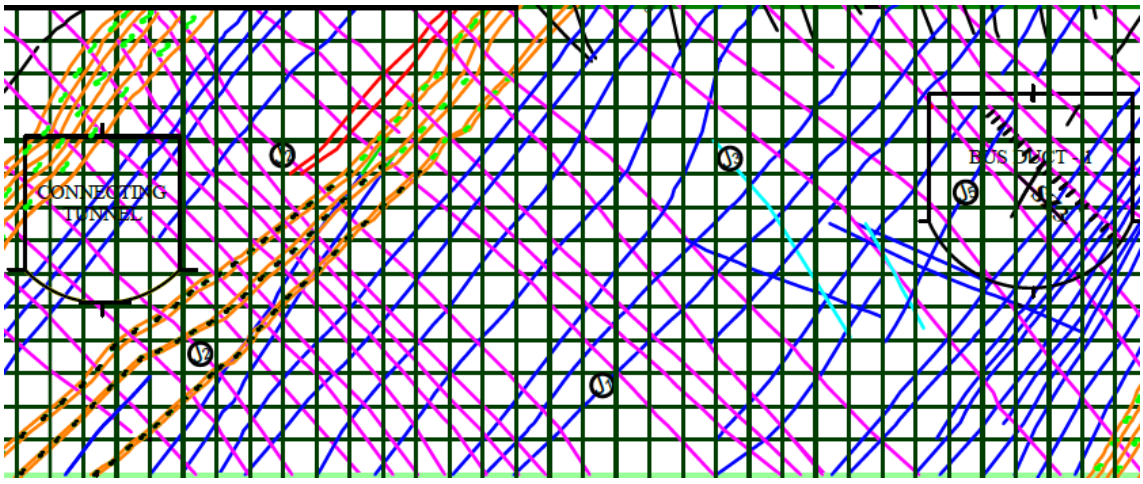

Fig.15. Geological log downstream wall of the machine hall between connecting tunnel and Bus-duct-1

zone may reactivate the local fault and result in rockmass failure (Blenkinsop 2008; Virgo *et al.* 2014; Laubach *et al.* 2018; Moore and Lockner 1995).

TVHPP powerhouse has been constructed in a geologically complex zone having seismically active environment. There are five major joints namely J1, J2, J3, J4 and J5 and six shear zones namely SZ1, SZ2, SZ3, SZ4, SZ5 and SZ6 in the downstream wall of the powerhouse (figure 14).

Microseismic data analysis showed that though the number of larger magnitude events were less but smaller magnitude events were more frequent even after the completion of the powerhouse. Mcgarr displacement is observed highest in Zone A. This zone falls between connecting tunnel and bus duct-1. Using Gutenberg Richter relationship for the occurrences of the events between the connecting tunnel and bus duct-1, b-value is 1.49. The parameter-b is high for this zone because occurrence of micro-cracks in this zone is more as compared to the entire powerhouse (b is 0.56 for complete powerhouse). It might be because the portion of joints J1, J2, J3 and J5; and shear zone SZ3 in the downstream wall of the machine hall adjacent to bus duct-1 and connecting tunnel are quite active (figure 15). This zone may be potentially unstable and it needs extra stability measures.

CONCLUSIONS

The present study is based on the real time microseismic monitoring of the powerhouse of TVHPP hydropower project in the Uttrakhand Himalayan region. This network was able to provide three-dimensional picture of fracture/ micro-crack propagation with time and potential hazardous zone. One hundred seventy eight microseismic events were recorded which were subjected to thorough temporal and spatial analysis and interpretation to understand the underground powerhouse rockmass strata stability.

Temporal analysis states that deformation has decreased with time which indicates a stable underground powerhouse rockmass cavern. However, there are probability of occurrences of high local magnitude with time in and around the powerhouse, so underground cavern rockmass is under threat.

Source parameters of these microseismic events provided vital information of the spatial and temporal distribution of events and their correlation to the existing geological features in the powerhouse. An attempt was made to correlate the microseismic activity with the stability of the underground rockmass structure and existing geological features in the cavern. Most of the microseismic activities were located between connecting tunnel and bus duct 1 (Zone -A).

Since the most active seismic zone is located between connecting tunnel and bus duct 1, it is concluded that the portion of joints and shear zone in the downstream wall of the machine hall adjacent to this connecting tunnel and bus-duct-1 were active. They need extra stability measures (rock bolting) to prevent further deterioration.

Acknowledgement: This study is based on the Microseismic monitoring study conducted at TVHPP. The authors are grateful to the Director, National Institute of Rock Mechanics for the necessary support and approval to publish these findings. The authors are also grateful to the Management (for sponsoring, logistic and access for this study) and staff at TVHPP NTPC Ltd. Special thanks are due to

Mr. N. Gopalakrishnan, DGM, NTPC Ltd. for providing the requisite site literature and other logistic support at site during the monitoring period. Help from colleagues of NIRM is also acknowledged. An honest thanks to Dr. Iram Saba Amin for proof-reading.

References

Aswegen G. Van, Mendecki, A.J., Lachenicht, R., Dzhafarov, A. H., Hofmann, Radu, G.S., Eneva, M., Sciocatti, M. and Kotze, G. (1999) Mine layout , geological features and seismic hazard, GAP-303, ISS International Limited, http://researchspace.csir.co.za/dspace/bitstream / handle/10204/1697/gap303.pdf;jsessionid=5E3E7DAD5E53D25B88C45BCCAB5EA669?sequence=1.

Aswegen G. Van and Butler, A.G. (1993) Applications of quantitative seismology in South African gold mines. Proc. 3rd Internat. Symp. Rockbursts and Seismicity in Mines. Rotterdam: AA Balkema, pp.261–266.

Blenkinsop, T. G. (2008) Relationships between faults, extension fractures and veins, and stress. Jour. Struct. Geol., v.30/5, pp.622–632. DOI: 10.1016/j.jsg.2008.01.008

Bormann, P., Baumbach, M., Bock, G., Grosser, H., Choy, G. L., & Boatwright, J. (2009) Seismic sources and source parameters. Geo Forschungs Zentrum (Ed.) New manual seismological observatory practice, vol 1, pp. 1–94. Potsdam.

Butler, G.V.A. and Van, A.G. (1993) Applications of quantitative seismology in South African gold mines'. Proc.e 3rd Internat. Symp. on Rock bursts and Seismicity in Mines. Rotterdam: AA Balkema, pp.261–266.

Caving, S. and Potvin, Y. (2008) Seismic monitoring of the Northparkes lift 2 block cave - Part 1 Undercutting. South African Institute of Mining and Metallurgy, July, pp335–354.

Chen, F., Ma, T., Tang, C., Du, Y., Li, Z. and Liu, F. (2018) 'Research on the Law of Large-Scale Deformation and Failure of Soft Rock Based on Microseismic Monitoring. Advan. Civil Engg., v.8. DOI: 10.1155/2018/9286758

Dai, F., Li, B., Xu, N., Zhu, Y. and Xiao, P. (2015) Stability evaluation on surrounding rocks of underground powerhouse based on microseismic monitoring. Shock and Vibration, v.9. DOI: 10.1155/2015/937181

Dunnicliff, J. (1982) Geotechnical Instrumentation for monitoring field performance. Washington.

Emsley, S., Olsson, O., Stenberg, L., Alheid, H. and Falls, S. (1997) *ZEDEX-A study of damage and disturbance from tunnel excavation by blasting and tunnel boring*. Retrieved from <http://inis.iaea.org/search/search.aspx?orig_q=RN:29050588>

Enrique, Rubio and Daulat, N. (2007) Caving performance through the integration of microseismic activity and numerical modeling at DOZ-PT freeport, Indonesia. Erik Eberhardt, Doug Stead T.M. (Eds.) First Canada-U.S. Rock Mechanics Symposium. Taylor & Francis.

Esso Highlands Limited (2006) Environmental Assessment Report, Papua New Guinea: PNG Gas Project, Vol. 26.

Essrich, F. (2005) Mine Seismology for Rock Engineers–An Outline of Required Competencies. Proc. Sixth Internat. Symp. on Rockbursts and Seismicity in Mines, pp.359–364.

Finno, R.J. (1991) Geotechnical instrumentation for monitoring field performance. Engg. Geol., v.30/2, pp.237–238. Elsevier BV. DOI: 10.1016/0013-7952(91)90045-m

Glazer, S.N. (2018) Mine seismology: Seismic response to the caving process: A case study from four mines. Mine Seismology: Seismic Response to the Caving Process: A Case Study from Four Mines. Springer International Publishing. DOI: 10.1007/978-3-319-95573-5

Gutenberg, B. and Richter, C.F. (1956) Magnitude and energy of earthquakes. Annali di Geofisica, v.9/1, pp.7–12. DOI: 10.4401/ag-4588

Hudyma, M.R. (2008) Analysis and interpretation of clusters of seismic events in mines. University of Western Australia.

Laubach, S.E., Lamarche, J., Gauthier, B.D. M., Dunne, W.M. and Sanderson, D. J. (2018) Spatial arrangement of faults and opening-mode fractures. Jour. Struct. Geol., v.108, pp.2–15. Elsevier Ltd. DOI: 10.1016/j.jsg.2017.08.008

Li, B., Xu, N., Dai, F., Zhang, G. and Xiao, P. (2019).Dynamic analysis of rock mass deformation in large underground caverns considering microseismic data. Internat. Jour. Rock Mechanics and Mining Sciences, 122/August: 13. Elsevier Ltd. DOI: 10.1016/j.ijrmms.2019.104078

Madariaga, R. (1989) Seismic source: Theory. Geophysics, pp. 1129–33. Springer US: Boston, MA. DOI: 10.1007/0-387-30752-4_137

Martin, C.D., Kaiser, P.K. and Christiansson, R. (2003) Stress, instability and design of underground excavations', Internat. Jour. Rock Mechanics and Mining Sciences, v.40/7–8, pp.1027–47. DOI: 10.1016/S1365-1609(03)00110-2

McGarr, A. and Fletcher, J.B. (2003) Maximum slip in earthquake fault zones, apparent stress, and stick-slip friction. Bull. Seismolog. Soc. Amer., v.93/6, pp.2355–2362. DOI: 10.1785/0120030037

Mcgarr, A. (1991) Observations Constraining Near-Source Ground Motion Estimated From Locally Recorded Seismograms. Jour. Geophys. Res., v.96/16, pp.495–508.

Mendecki, A.J. (2012) Size Distribution of Seismic Events in Mines. Australian Earthquake Engg. Soc., p. 20. Queensland.

Mendecki, A.J. (2015) Mine Seismology Reference Book Seismic Hazard. Institute of Mine Seismology.

Mendecki A.J., Lynch, R.A. and Malovichko, D.A. (2010) Routine Micro-Seismic Monitoring in Mines. Australian Earthquake Engg. Soc., pp. 1–33. Perth.

Moore, D.E. and Lockner, D.A. (1995) The role of microcracking in shear-fracture propgation in granite. *Jour. Struct. Geol.*, v.17/1, pp.95–114. DOI: 10.1016/0191-8141(94)E0018-T

Naithani, A.K. and Murthy, K.S.K. (2006) Geological and geotechnical investigations of Tapovan – Vishnugad Hydroelectric Project, Chamoli District, Uttarakhand, India. Jour. Nepal Geol. Soc., January 2006.

Sujit Dasgupta, Prabhash Pande, Dhruba Ganguly, Zafae Iqbal, Kanika Sanyal, N.V. Venkataraman, Sabyasachi Dasgupta, Basudev Sural, L. Harendranath, K. Mazumdar, Satrajit Sanyal, A. Roy, L. K. Das, P. S. M. and H. K. G. (2000) Seismotectonic Atlas of India and its Environs.

van Aswegen, G., Mendecki, A.J., Lachenicht, R., Dzhafarov, A.H., Hofmann, G., Radu, S., Eneva, M., Sciocatti, M. and Kotze, G. (1999) Mine layout, geological features and seismic hazard.

Vikalp Kumar, N. Gopalakrishnan, N.P.S. and S.C. (2019) 'Microseismic monitoring application for primary stability evaluation of the powerhouse of the Tapovan Vishnugad Hydropower Project. Jour. Earth System Sci., v.128/6. DOI: 10.1007/s12040-019-1191-9

Virgo, S., Abe, S. and Urai, J.L. (2014) The evolution of crack seal vein and fracture networks in an evolving stress field: Insights from Discrete Element Models of fracture sealing. Jour. Geophys. Res.: Solid Earth, v.119/12, pp.8708–8727. DOI: 10.1002/2014JB011520

Vyshnavi, S., Islam, R. and Sundriyal, Y. P. (2015) Comparative study of soil profiles developed on metavolcanic (basaltic) rocks in two different watersheds of Garhwal Himalaya. Curr. Sci., v.108/4, pp.699–707. DOI: 10.18520/cs/v108/i4/699-707

Xiao, P., Li, T., Xu, N., Zhou, Z. and Liu, X. (2019) Microseismic monitoring and deformation early warning of the underground caverns of Lianghekou hydropower station, Southwest China. Arabian Jour. Geosci., v.12/16, pp.18. DOI: 10.1007/s12517-019-4683-7

Xiao, P., Qian, B., Jiang, P., Xu, N. and Li, B. (2018) Deformation Forecasting of Surrounding Rock Mass Based on Correlation between Frequency and Fracture Scale of Microseismicity. Advan. Civil Engg., 2018. DOI: 10.1155/2018/4037402

(Received: 18 July 2020; Revised form accepted: 6 May 2021)